

MOL 8730

Superagonistic action of 14-epi-analogs of 1,25-Dihydroxyvitamin D Explained by Vitamin D Receptor – Coactivator Interaction

Guy Eelen, Lieve Verlinden, Natacha Rochel, Frank Claessens, Pierre De Clercq,
Maurits Vandewalle, Giuseppe Tocchini-Valentini, Dino Moras, Roger Bouillon and
Annemieke Verstuyf

Laboratorium voor Experimentele Geneeskunde en Endocrinologie, Katholieke
Universiteit Leuven, B-3000 Leuven, Belgium (GE, LV, RB, AV)

Département de Biologie et de Génomique Structurales, IGBMC, CNRS/
INSERM/Université Louis Pasteur, F-67404 Illkirch Cedex, France (NR, DM)

Afdeling Biochemie, Gasthuisberg, Katholieke Universiteit Leuven, B-3000 Leuven,
Belgium (FC)

Vakgroep voor Organische Chemie, Universiteit Gent, B-9000 Gent, Belgium (PDC,
MV)

Istituto di Biologia Cellulare, Consiglio Nazionale delle Ricerche, Campus A. Buzzati-
Traverso, Via Ramarini, 32, 00016 Monterotondo Scalo, Rome, Italy (GT-V; current
address)

Running title: Enhanced coactivator recruitment by 14-epi-vitamin D-analogs

Corresponding author to whom reprint request should be addressed;

Roger Bouillon, PhD, MD

Laboratorium voor Experimentele Geneeskunde en Endocrinologie

Onderwijs en Navorsing, Gasthuisberg

Herestraat 49, B-3000 Leuven, Belgium

Tel.: +32-16-345970

Fax: +32-16-345934

E-mail: roger.bouillon@med.kuleuven.ac.be

Number of text pages (including references, footnotes and figure legends): 28

Number of tables: 1

Number of figures: 8

Number of references: 29

Number of words in the abstract: 249

Number of words in the introduction: 643

Number of words in the discussion: 1484

Nonstandard abbreviations: 1,25-(OH)₂D₃, 1,25-dihydroxyvitamin D₃; DRIP, vitamin-D-receptor interacting protein; LBD, ligand binding domain; SRC, steroid receptor coactivator; TIF, transcriptional intermediary factor; TX522, 19-nor-14-epi-23-yne-1,25-(OH)₂D₃; TX527, 19-nor-14,20-bisepi-23-yne-1,25-(OH)₂D₃; VDR, vitamin D receptor; VDRE, vitamin D response element

Abstract

Two 14-epi-analogs of 1,25-dihydroxyvitamin D₃ [1,25-(OH)₂D₃], 19-nor-14-epi-23-yne-1,25-(OH)₂D₃ (TX522) and 19-nor-14,20-bisepi-23-yne-1,25-(OH)₂D₃ (TX527), show enhanced antiproliferative (at least 10-fold) and markedly lower calcemic effects both *in vitro* and *in vivo*, when compared with 1,25-(OH)₂D₃. This study aimed to evaluate their superagonistic effect at the level of interaction between the Vitamin D Receptor (VDR) and coactivators. Mammalian two-hybrid assays with VP16-fused VDR and GAL4-DNA-Binding-Domain-fused SRC-1, TIF2 or DRIP205 showed the 14-epi-analogs to be more potent inducers of VDR – coactivator interactions than 1,25-(OH)₂D₃ (up to 16- and 20-fold stronger induction of VDR-SRC-1 interaction for TX522 and TX527 at 10⁻¹⁰ M). Similar assays in which metabolism of 1,25-(OH)₂D₃ was blocked with VID400, a selective inhibitor of the 1,25-(OH)₂D₃-metabolizing enzyme CYP24, showed that the enhanced potency of these analogs in establishing VDR-coactivator interactions can only partially be accounted for by their increased resistance to metabolic degradation. Crystallization of TX522 complexed to the Ligand Binding Domain (LBD) of the human VDR demonstrated that the epi-configuration of C14 caused the CD ring of the ligand to shift by 0.5 Å thereby bringing the C12 atom into closer contact with Val300. Moreover, C22 of TX522 made an additional contact with the CD1 atom of Ile268 due to the rigidity of the triple bond-containing side chain. The position and conformation of the activation helix H12 of VDR was strictly maintained. In conclusion, this study provides deeper insight into the docking of TX522 in the LBP and shows that stronger VDR – coactivator interactions underlie the superagonistic activity of the two 14-epi-analogs.

Introduction

1,25-Dihydroxyvitamin D₃ [1,25-(OH)₂D₃], the biologically active form of vitamin D, plays a major role in bone metabolism and in calcium and phosphate homeostasis. In addition to this classic effect, 1,25-(OH)₂D₃ also has an antiproliferative and prodifferentiating effect on various normal as well as malignant cells (Bouillon *et al.*, 1995). This makes 1,25-(OH)₂D₃ a candidate drug for cancer treatment. However, at the pharmacological doses needed for this application, 1,25-(OH)₂D₃ displays major calcemic side-effects (e.g. hypercalcemia and hypercalciuria). Hence the effort to design analogs of 1,25-(OH)₂D₃ with a clear dissociation between antiproliferative and calcemic effects. Two of these analogs, the 14-epi-analogs TX527 and TX522 (Fig. 1) show a strongly enhanced antiproliferative action (at least 10-fold) coupled to markedly lower calcemic effects (50 to 400 times less than 1,25-(OH)₂D₃ respectively) and fulfil the profile needed for therapeutic application (Verlinden *et al.*, 2000). The reason why TX522 and TX527 have a superagonistic effect compared to their parent compound remains to be determined.

In a previous study we aimed to clarify the molecular mode of action of these two analogs and demonstrated that there was no difference between them and 1,25-(OH)₂D₃ at the level of binding of the different ligands to the vitamin D receptor (VDR) nor at the level of the binding between the ligand-bound VDR and its preferred dimerization partner, the retinoid X receptor (RXR). Moreover, it was shown that the profile of the analogs could not be explained by the interaction between the VDR-RXR heterodimer and its target DNA sequences (VDREs) (Verlinden *et al.*, 2001). The next step in the transcriptional process is the recruitment of coregulator molecules to the ligand-bound

VDR. The abovementioned findings point towards a possible key role for these coregulator molecules in the elucidation of the superagonistic action of the analogs.

The function and the importance of coregulators, comprising both coactivators and corepressors, in nuclear receptor-mediated gene transcription have been described at length. Coactivators interacting with the VDR include the p160 family members such as SRC-1, GRIP1/TIF2 and ACTR (reviewed by Rachez and Freedman, 2000). These coactivators recruit histone acetyl-transferase (HAT)-activity and create a permissive chromatin surrounding for gene transcription by acetylation of histone tails. A distinct type of coactivator for the VDR is the multi-protein complex DRIP, the 205 kDa subunit of which was proven to interact directly with the ligand binding domain (LBD) of the VDR and to anchor other subunits of the complex to the receptor. When bound to the liganded VDR, the DRIP complex is believed to enhance transcription by binding to RNA polymerase II and thus by recruiting the basal transcription machinery to the promoter (Rachez *et al.*, 1998, 1999, 2000).

To elucidate the molecular mechanism behind the superagonistic profile of the two 14-epi-analogs TX522 and TX527, this study aims to investigate the influence of 1,25-(OH)₂D₃ and the two analogs on the interaction between the VDR and different coactivator molecules including SRC-1, TIF2 and the 205 kDa subunit of the DRIP complex (DRIP205). Mammalian two-hybrid studies with VP16-fused VDR (pVPVDR) and GAL4-DBD-fused SRC-1, TIF2 or DRIP205 in COS1 cells treated with TX522 or TX527 revealed stronger interactions between VDR and each of the three coactivators than in cells treated with 1,25-(OH)₂D₃. Selective inhibition of the 24-hydroxylase enzyme (CYP24), which is the main enzyme involved in the catabolism of 1,25-(OH)₂D₃,

showed that these differences can only partially be accounted for by a difference in metabolic stability between 1,25-(OH)₂D₃ and the two analogs. Resolution of the crystal structure of the human VDR-LBD in complex with TX522 revealed modified contacts of C12 and C22 of the ligand with the Ligand Binding Pocket (LBP)-lining residues Val300 and Ile268 respectively. These data show the existence of subtle differences in ligand docking between 1,25-(OH)₂D₃ and a 14-epi-analog. In addition, enhanced coactivator binding by VDR was shown to be the explanation at the molecular level for the superagonistic activity of TX522 and TX527.

Materials and methods

Plasmids and reagents

The GAL4 DNA-binding domain cloning vector pM, the activation-domain cloning vector pVP16 and the reporter construct pG5CAT are part of the Mammalian Matchmaker Two-Hybrid Assay kit (Clontech, Erembodegem, Belgium). The pVPVDR construct was made by cloning the 1284bp fragment of the pAS2VDR construct, which was obtained from D. Feldman (Stanford University School of Medicine, Stanford, CA, USA), into the pVP16 vector using the *Bam*HI and *Sal*I restriction sites. To make the pMDRIP205 construct, a fragment of DRIP205 (AA 510-787) was generated by PCR with the forward primer 5'-CGCGGATCCCACTGTCCCTCATTGCAGAG-3' and the reverse primer 5'-TGCTCTAGAGGCTGGGCAATCATCACTA-3'. The fragment was subcloned into the *Bam*HI and *Xba*I restriction sites of the pM vector. The GAL4 DNA-binding domain containing constructs pGALTIF2.4 (AA 624-1010) and pSG424SRC1NIR (AA 570-782) were obtained from H. Gronemeyer (IGBMC, CNRS/INSERM/ULP, Illkirch, France) and M.G. Parker (Imperial Cancer Research Fund, London, UK) respectively.

1,25-(OH)₂D₃ was obtained from J.P. van de Velde (Solvay, Weesp, The Netherlands). The 14-epi-analogs 19-nor-14-epi-23-yne-1,25-(OH)₂D₃ (TX522) and 19-nor-14,20-bisepi-23-yne-1,25-(OH)₂D₃ were originally synthesized by M. Vandewalle and P. De Clercq from the University of Ghent (Belgium) and were obtained from Théraxem S.A. (Monaco) (Verlinden *et al.*, 2000). MC903 and KH1060 were a gift from L. Binderup (Leo Pharmaceuticals, Ballerup, Denmark). Ro24-5531 was kindly provided by M.

Uskokovic (Hoffmann-La Roche, Nutley, NJ). The 24-hydroxylase inhibitor VID400 was obtained from A. Stütz (Novartis, Vienna, Austria).

Transient transfection assays

COS-1 cells (ATCC, Manassas, VA, USA) were maintained in DMEM containing 10% fetal bovine serum (Biochrom KG, Berlin, Germany) supplemented with glutaMAX-I, 100U/ml penicillin and 100 µg/ml streptomycin (Invitrogen, Merelbeke, Belgium). Approximately 1.5×10^5 cells were seeded 24 hours prior to transfection in 6-well plates. Cells were transfected with DOTAP Liposomal Transfection Reagent (Roche Diagnostics, Mannheim, Germany) as specified by the manufacturer. The amounts of plasmid DNA used for transfection were 300 ng for the GAL4-fusion, 300 ng for the VP16-fusion and 1.5 µg for the CAT-reporter plasmid. Cells were treated with 1,25-(OH)₂D₃, TX522, TX527, VID400 or vehicle (ethanol) 24 hours after transfection. CAT-amounts were assayed 24 hours thereafter with a CAT-ELISA (Roche Diagnostics) according to the manufacturer's instructions and were corrected for total protein contents.

Cell proliferation assays

As a measure of cell proliferation, [³H]-thymidine incorporation of breast cancer MCF-7 cells (ATCC) was determined after a 72-h incubation period with various concentrations of 1,25-(OH)₂D₃, analogs or vehicle as described previously (Verstuyf *et al.*, 1998).

Crystallography

Expression, purification and crystallization

The LBD of the human VDR (residues 118-427 Δ 165-215) was cloned in pET28b expression vector, to obtain an N-terminal hexahistidine-tagged fusion protein, and overproduced in *E. Coli* BL21 (DE3) strain. Cells were grown in LB medium and subsequently induced for 6 h at 20°C with 1 mM isopropyl thio- β -D-galactoside. The purification included a metal affinity chromatography step on a cobalt-chelating resin. After tag removal by thrombin digestion, the protein was further purified by gel filtration. The final protein buffer was 10 mM Tris pH 7.5, 100 mM NaCl, 5 mM dithiothreitol. The protein was concentrated to 10 mg/ml and incubated in the presence of 5 fold molar excess of ligand. Purity and homogeneity were assessed by SDS and native PAGE and denaturant and native electrospray ionization mass spectrometry. Crystals of the different complexes were obtained at 4°C by vapor diffusion in hanging drops with reservoir solutions containing 0.1 M Mes pH 6.0, and 1.4 M ammonium sulfate and appeared after 4 days.

X-ray Crystallography Data Collection and Processing

Crystals were mounted in capillary. One single native data set was collected for each complex at 4°C at the beamline BM14 of the European Synchrotron Radiation Facility (Grenoble, France). Data were processed using the program HKL2000 (Otwinowski and Minor, 1997).

Structure Determination and Refinement

Initial phase estimates were obtained by omitting the 1,25-(OH)₂D₃ from the structure of the VDR-1,25-(OH)₂D₃ complex previously solved. After a rigid body refinement with

CNS (Brunger *et al.*, 1998) the refinement proceeded performing iterative cycles of least-squares minimization and manual model building using the program O (Jones *et al.*, 1991). The ligand molecules were only included at the last stage of the refinement. Anisotropic scaling and a bulk solvent correction were used. Individual B atomic factors were refined anisotropically. Solvent molecules were then placed according to unassigned peaks in the difference Fourier maps. All of the refined models showed unambiguous chirality for the ligands and no Ramachandran plot outliers according to procheck. The volumes of the ligand-binding pockets and ligands were calculated as previously reported.

Protein Data Bank Accession Number

The accession number for the coordinates of the structure VDR-TX522 reported in this article is 1TXI.

Results

Effects of 1,25-(OH)₂D₃ and 14-epi-analogs on the interaction between VDR and coactivator molecules

To determine the effect of 1,25-(OH)₂D₃ and the two 14-epi-analogs TX522 and TX527 on the interaction between VDR and the coactivator Transcriptional Intermediary Factor 2 (TIF2), a mammalian two-hybrid system with a VP16-fused VDR (pVPVDR), a GAL4-DNA binding domain-fused TIF2.4 (pGALTIF2.4) and a chloramphenicol-acetyltransferase-reporter construct (pG5CAT) were used. In order to exclude any possible bias caused by the two activation domains of TIF2 (AD1 and AD2), the coactivator fragment TIF2.4 (AA 624-1010) was used. This fragment contains the Nuclear Receptor Interacting Domain (NID) but lacks AD1 and AD2. Transient transfection of the abovementioned plasmids into COS1 cells and subsequent treatment of these cells with 1,25-(OH)₂D₃, TX522 or TX527 yielded clear differences in CAT-reporter gene expression (Fig. 2). Cells treated with 10⁻¹⁰ M and 10⁻⁹ M TX522 or TX527 had clearly higher VDR – TIF2.4 interaction [1.6- and 2.3-fold respectively for TX522; 2.7- and 2.7-fold respectively for TX527] than cells treated with 1,25-(OH)₂D₃ at the same doses. At 10⁻⁸ M only TX527 induced a significantly higher VDR – TIF2.4 interaction; at 10⁻⁷ M there was no more difference between 1,25-(OH)₂D₃ and either of the two analogs. TX522 required approximately 10-fold lower concentrations than 1,25-(OH)₂D₃ for the induction of half-maximal VDR – TIF2.4 interaction, whereas TX527 required approximately 20- to 50-fold lower concentrations for the same induction. Cotransfection of either pVPVDR or pGALTIF2.4 alone together with pG5CAT and

subsequent treatment with 1,25-(OH)₂D₃, TX522 or TX527 did not yield significant or ligand-dependent reporter gene expression (data not shown).

Similar experiments were performed with the coactivator Steroid Receptor Coactivator 1 (SRC-1) and again a fragment of the coactivator (AA570-782; pSG424SRC1NIR), which contains the Nuclear Receptor Interacting Domain but lacks AD1 and AD2, was used. Even at 10⁻¹¹ M, the 14,20-bisepi-analog TX527 caused a 6-fold higher VDR – SRC-1 interaction than 1,25-(OH)₂D₃ and at 10⁻¹⁰ M a 16- and 20-fold stronger interaction was observed in TX522- and TX527-treated samples (Fig. 3). In cells treated with 10⁻⁹ M TX522 and TX527 VDR – SRC-1 interaction was clearly, though statistically not significantly, higher than in 1,25-(OH)₂D₃-treated samples. At 10⁻⁸ M there was no longer a difference between 1,25-(OH)₂D₃ and either of the analogs. Based on the half-maximal induction of VDR – SRC-1 interaction, TX522 and TX527 are both at least 10 times more potent than 1,25-(OH)₂D₃. Cotransfection of either pVPVDR or pSG424SRC1NIR alone together with pG5CAT and subsequent treatment with 1,25-(OH)₂D₃, TX522 or TX527 did not yield significant or ligand-dependent reporter gene expression (data not shown).

Next, a third coactivator, namely DRIP205, was used which is devoid of HAT-activity but instead is part of a larger DRIP complex which recruits RNA polymerase II. A fragment (AA 510-787) containing the two nuclear receptor interaction motifs NR1 and NR2 was fused to the GAL4-DBD (pMDRIP205) and cotransfected with pVPVDR and pG5CAT in COS1 cells which were then treated with the different ligands (Fig. 4). At 10⁻¹⁰ M, TX522 and TX527 induced a 4- and 10-fold higher VDR – DRIP205 interaction than 1,25-(OH)₂D₃. These differences increased to 6-fold for TX522 and stayed at 10-

fold for TX527 at 10^{-9} M and dropped to 2- and 2.6-fold for TX522 and TX527 respectively at 10^{-8} M. TX522 and TX527 require 30- and 40-fold lower doses to obtain the VDR – DRIP205 interaction induced by 1,25-(OH) $_2$ D $_3$ at 10^{-8} M. Cotransfection of either pVPVDR or pMDRIP205 alone together with pG5CAT and subsequent treatment with 1,25-(OH) $_2$ D $_3$, TX522 or TX527 did not yield significant or ligand-dependent reporter gene expression (data not shown).

Metabolism of 1,25-(OH) $_2$ D $_3$ and 14-epi-analogs; effect on VDR-coactivator interaction

The parent compound 1,25-(OH) $_2$ D $_3$ is mainly metabolized by the 24-hydroxylase-pathway whereas the two 14-epi-analogs have a 23-yne structure that prevents them from being metabolized through the same pathway. The observed differences in interaction between VDR and coactivators in 1,25-(OH) $_2$ D $_3$ -treated samples and samples treated with TX522 or TX527 might therefore be due to different rates of metabolism through the 24-hydroxylase-pathway for 1,25-(OH) $_2$ D $_3$ and the two analogs. Therefore, we determined the importance of this difference in metabolism and evaluated the intrinsic potency of 1,25-(OH) $_2$ D $_3$ to induce VDR – coactivator interactions, unbiased by 24-hydroxylase-mediated metabolism. To do so, COS1 cells were transfected with pVPVDR, pMDRIP205 and the CAT-reporter construct, treated with 2×10^{-7} M VID400, which is a selective inhibitor of the 24-hydroxylase enzyme (CYP24) (Schuster *et al.*, 2001a,b), and treated with 1,25-(OH) $_2$ D $_3$, TX522 or TX527 at 10^{-9} M (Fig. 5). For 1,25-(OH) $_2$ D $_3$ a 3-fold increase in VDR – DRIP205 interaction was seen in cells treated with VID400 as compared with treatment without VID400. As could be expected, addition of

VID400 did not yield any significant changes in VDR – DRIP205 interaction for TX522- or TX527-treated samples. At 10^{-9} M of the different ligands, differences in VDR – DRIP205 interaction between 14-epi-analogs and 1,25-(OH) $_2$ D $_3$ diminished after addition of VID400 but remained significant. Growth inhibition in MCF-7 breast cancer cells after combined treatment with 1,25-(OH) $_2$ D $_3$, TX522 or TX527 and VID400, reflected these findings (Fig. 6). The EC $_{50}$ value for 1,25-(OH) $_2$ D $_3$ for half maximal [3 H]-thymidine incorporation shifted from 1.1×10^{-7} M to 1.0×10^{-8} M when VID400 was added to the cells. In contrast, the shifts in EC $_{50}$ values for TX522 and TX527 after addition of VID400 were only 2.5- and 1.5-fold, respectively.

Crystal structure of VDR-TX522

To obtain crystals of the hVDR LBD complexes we used a hVDR LBD mutant lacking 50 residues in the loop connecting helices H2 and H3. The same construct was previously used to solve the structure of the hVDR LBD bound to 1,25-(OH) $_2$ D $_3$ and to several synthetic ligands (Rochel *et al.*, 2000; Tocchini-Valentini *et al.*, 2001, 2004). This mutant has the same biological properties (binding, transactivation in several cell lines, heterodimerization) as the hVDR LBD wild-type (Rochel *et al.*, 2001). The crystals were obtained in similar conditions and were isomorphous. The structure of VDR-TX522 has been refined at a resolution of 1.9 Å. The experimental data and refinement statistics are summarized in Table 1. After refinement of the protein alone, the map shows an unambiguous electron density where to fit the ligand.

The hVDR LBD complexes adopt the canonical conformation of all previously reported agonist-bound nuclear receptor LBDs with 12-13 α -helices organized in a 3 layered

sandwich. In all the structures of hVDR bound to agonist ligands, a single conformation of the complex is observed. The position and conformation of the activation helix H12 is strictly maintained. The ligands adopt the same orientation in the pocket (Fig. 7). An adaptation of their conformation is observed in order to maintain the hydrogen bonds forming the anchoring points. When compared to the structure of hVDR-1,25-(OH)₂D₃ complex, the atomic models of hVDR bound to TX522 show rms deviations of 0.39 Å on all atoms. The ligand is buried in the predominantly hydrophobic pocket that is conserved in all complexes. The sizes of the ligands are 381 Å³ and 374 Å³ for 1,25-(OH)₂D₃ and TX522, respectively. The volume of the ligand binding cavity is 660 Å³ and the two ligands occupy 57 % of the pocket.

The interactions between the ligands and the receptor involve hydrophobic contacts and electrostatic interactions. The A, secoB rings present similar conformations as the natural ligand (Fig. 7). Due to the epi-configuration of C14, the CD rings are shifted by 0.5 Å. The distance between the C12 atoms of TX522 and 1,25-(OH)₂D₃ is 0.5 Å. Due to the triple bond of the side chain and the reversed configuration of C14, the C21 atom is shifted by 0.4 Å. The distance between the 1-hydroxy and the 25-hydroxy groups varies from 13.3 Å for TX522 and 13.0 Å for 1,25-(OH)₂D₃ complex. All the residues forming the binding pocket adopt the same conformation as in the VDR-1,25-(OH)₂D₃ structure. All contacts between the ligand and the protein observed in the VDR-1,25-(OH)₂D₃ are maintained in the VDR-TX522 complex. The C12 shift induces a closer contact of this atom to Val300 (H6) in the VDR-TX522. Due to its rigidity, the side chain of TX522 takes another pathway in the pocket and makes an additional contact with the CD1 atom of Ile268 (H5) at 3.7 Å of C22 atom instead of 4.3 Å for 1,25-(OH)₂D₃ (Fig. 8).

Discussion

Ever since the discovery of the antiproliferative and prodifferentiating action of 1,25-(OH)₂D₃ in the 1980s, efforts have been made to develop superagonistic analogs of 1,25-(OH)₂D₃ with a dissociation between the antiproliferative effect and the calcemic side effects (Bouillon *et al.*, 2003). The two 14-epi-analogs TX522 and TX527 display markedly enhanced antiproliferative potencies coupled to reduced calcemic effects. Our previous attempts to unravel the superagonistic profile of these two analogs at the level of their molecular mode of action have demonstrated that the superagonism is not due to enhanced binding to the VDR, nor to differences at the level of heterodimerization between ligand-bound VDR and RXR, nor to enhanced binding of the VDR-RXR heterodimer to VDREs (Verlinden *et al.*, 2001). These findings led to the hypothesis that the specific profile of these analogs might be explained at the next level of transcriptional regulation by 1,25-(OH)₂D₃, namely the recruitment of coactivator molecules. Recent studies describe the effect of different analogs of 1,25-(OH)₂D₃ on the interaction of VDR with coactivators (Takeyama *et al.*, 1999; Issa *et al.*, 2002). The present study investigates the 14-epi-analogs TX522 and TX527 and their influence on VDR-mediated recruitment of the coactivators TIF2, SRC-1 and DRIP205. A stronger induction of the interaction between VDR and each of the three coactivators was observed in cells treated with TX522 or TX527 when compared with 1,25-(OH)₂D₃-treated cells. For TIF2 the higher induction was most obvious at 10⁻⁹ M and 10⁻¹⁰ M of the different ligands, for SRC-1 at 10⁻¹⁰ M and 10⁻¹¹ M and for DRIP205 at 10⁻⁸ M, 10⁻⁹ M and 10⁻¹⁰ M. On average, at least 10-fold lower doses than for 1,25-(OH)₂D₃ are sufficient for the two analogs to induce equivalent VDR – coactivator interactions. Similarly, a recent study with the

superagonistic analog 2-methylene-19-nor-(20*S*)-1,25-(OH)₂D₃ demonstrated this analog to be significantly more potent in inducing VDR interaction with SRC-1 and DRIP205 in a mammalian two-hybrid assay (Yamamoto *et al.*, 2003). ZK159222, a 25-carboxylic ester analog of 1,25-(OH)₂D₃ with antagonistic action, on the other hand, was found to be unable to induce interaction of the VDR with the coactivators TIF2, SRC-1 and RAC3 (Herdick *et al.*, 2000). Similar results were found for the 26,23-lactone TEI-9647 analog (Toell *et al.*, 2001). Taken together, our and others findings prove the ability of an analog to promote interaction between VDR and coactivator proteins to correlate well with the analogs superagonistic or antagonistic profile. In addition to TX522 and TX527 we used the analogs MC903, BL314, KH1060 and Ro24-5531 in the mammalian two-hybrid assay with VP16-fused VDR and GAL4DBD-fused TIF2.4 and found a strong correlation ($R^2=0.944$) for all six analogs between induction of VDR - TIF2.4 interaction and their potency to inhibit MCF-7 cell proliferation (unpublished data).

Metabolism of 1,25-(OH)₂D₃ in a cell occurs mainly via the 24-hydroxylation-pathway in which the 24-hydroxylase enzyme (CYP24) initiates metabolism by hydroxylation at C-24 of the side chain (Makin *et al.*, 1989; Reddy and Tserng, 1989). Other mechanisms of metabolism include C-23 and C-26 hydroxylation and C-3 epimerization. Making structural changes to the parent compound that render the molecule more resistant to this enzymatic metabolism, is a rational way to design 1,25-(OH)₂D₃-analogs. 20-epi- and 16-ene-analogs resist the 24-hydroxylation cascade and a 23-yne modification prevents analogs from being hydroxylated at C-23 and C-24 whereas fluorination of C-26 hampers 26-hydroxylation (Reddy *et al.*, 2000; Uskokovic *et al.*, 2001). Both 14-epi-analogs have a 23-yne structure, moreover, TX527 carries a 20-epi-modification. To determine

whether the enhanced potency of TX522 and TX527 to promote VDR-coactivator interactions is merely due to their 23-yne structure and the logically resulting increased resistance to 24-hydroxylase-mediated metabolic degradation and even more to estimate the actual potency of 1,25-(OH)₂D₃ – without influence of 24-hydroxylase-mediated metabolism – to induce VDR – coactivator interactions, the selective CYP24 inhibitor VID400 was used in the mammalian two-hybrid assay with pVPVDR and pMDRIP205. In samples treated with 1,25-(OH)₂D₃ but not in samples treated with TX522 or TX527, VDR-DRIP205 interaction increased 3-fold after addition of VID400. Despite this increase, the difference in potency to induce VDR – DRIP205 interaction between 1,25-(OH)₂D₃ and the two analogs remained significant. Growth inhibition assays on MCF-7 breast cancer cells treated with a combination of 1,25-(OH)₂D₃, TX522, TX527 and VID400 yielded comparable results. Addition of VID400 caused a 10-fold decrease in the EC₅₀ value for 1,25-(OH)₂D₃ while the decreases in the EC₅₀ value for TX522 and TX527 were only 2.5- and 1.5-fold. The resulting EC₅₀ value for 1,25-(OH)₂D₃, however, remained clearly higher than the EC₅₀ values for TX522 and TX527. The abovementioned findings demonstrate that differences in VDR-coactivator interaction could not completely be accounted for by different rates of metabolism through the 24-hydroxylase-pathway between 1,25-(OH)₂D₃ and the two analogs TX522 and TX527.

Another level at which the superagonistic profile of TX522 and TX527 can be explained would be the docking of the analogs in the LBD of the VDR and the possible subsequent conformational changes at the carboxyterminal helix 12 (H12) of the VDR which might influence coactivator binding. Upon ligand binding in the ligand binding pocket (LBP) of the LBD, H12, much like a mouse-trap, closes off the pocket and provides a surface upon

which coactivator molecules can bind through the LXXLL-motif in their nuclear receptor interacting domains. Superagonistic action of analogs, like for instance 20-epi-analogs, would then originate from conformational changes in the VDR-LBD which occur after docking of the analog in the LBP and which result in selective VDR-coactivator interaction and in an increased resistance of the VDR to proteolytic digestion. However, recent crystallographic studies of the VDR complexed to the natural ligand as well as to the superagonistic 20-epi-analogs MC1288 and KH1060 have clearly demonstrated that there is almost no difference in protein conformation between the LBD with 1,25-(OH)₂D₃ and the LBD with MC1288 or KH1060. (Rochel *et al.*, 2000; Tocchini-Valentini *et al.*, 2001). These findings support the idea of one single agonistic conformation of the VDR-LBP to which the different ligands adapt. A most recent study, however, demonstrates that, when complexed to a Gemini-analog with two side chains at C20 and an increase in volume of approximately 25% compared with 1,25-(OH)₂D₃, the conformation of the zebrafish VDR-LBD [the LBP lining residues of which show 100% identity with its human counterpart] adapts to this ligand and not the other way round (Ciesielski *et al.*, 2004). The superagonistic action of the 20-epi-analogs is likely to originate from more and stronger contact points with the LBP when compared to 1,25-(OH)₂D₃. Similarly, loss of interaction between oxygen-22 of the superagonistic 22-oxa-1,25-(OH)₂D₃ analog OCT and residues V234 and I268 of the LBP results in selective coactivator recruitment; interaction between VDR and TIF2 is promoted whereas SRC-1 and AIB-1 are not recruited by this analog (Takeyama *et al.*, 1999; Choi *et al.*, 2001). A recent study showed that the extended side chain of the abovementioned antagonist ZK159222 has steric contacts with A231 (H3) and V418 (H12) which result in

suboptimal position of H12 and almost complete loss of coactivator interaction (Tocchini-Valentini *et al.*, 2004). The two 14-epi-analogs under study, TX522 and TX527, might as well differ from the parent compound in the way they fit into the VDR-LBP. Additional or stronger interactions with residues of the LBP may well be the basis for their superagonistic action and increased potency to promote interaction between the VDR and the coactivators TIF2, SRC-1 and DRIP205. Crystallization of TX522 complexed to the VDR-LBD revealed that C12 of TX522 makes a closer contact with Val300 (H6) due to a shift of the CD-ring caused by the 14-epi-configuration. Moreover, the triple bond-containing side chain of TX522 is forced to select another pathway in the pocket thereby establishing an additional contact with the CD1 atom of Ile268 (H5). These closer and additional contacts between the analog and the LBP might cause TX522 to dissociate slower from the VDR than 1,25-(OH)₂D₃. In a previous study, however, we have shown that TX522 has a higher dissociation-rate than 1,25-(OH)₂D₃ (Verlinden *et al.*, 2001). A possible explanation for these seemingly contradicting findings can be that docking of a ligand in the VDR-LBP might be a much more dynamic process than can be shown by a static crystallography-based two-state, induced-fit model. However, transactivation studies with VDR constructs containing alanine-mutations in Ile268 or Val300 would be an appropriate tool to evaluate the importance of these two residues for docking of TX522 and subsequent transcriptional activity of the VDR. These two residues, however, are necessary for ligand binding and mutating them causes 1,25-(OH)₂D₃-induced transactivation to drop almost to the level of vehicle-induced transactivation. Differences between 1,25-(OH)₂D₃- and TX522-induced transactivation on these mutated VDRs therefore are difficult to detect (data not shown).

Cocrystallization studies of the VDR-LBD complexed to the natural ligand, TX522 or TX527 together with a coactivator molecule would be a possible way to unravel the superagonistic action of the 14-epi-analogs.

In conclusion, this study shows that the enhanced potency to induce VDR – coactivator interactions is the basis for the superagonistic profile of TX522 and TX527.

Acknowledgements

The authors like to thank M. Van Camp, B. K. Tan, S. Marcelis and R. Ponsaerts for excellent technical assistance as well as A. Mitschler and the staff of the beamline BM14 at the European Synchrotron Radiation Facility (ESRF, Grenoble, France) for technical assistance during data collection. The authors like to express their gratitude to Sachiko Yamada for providing the VDR alanine mutants.

Reference List

Bouillon R, Okamura WH and Norman AW (1995) Structure-Function Relationships in the Vitamin D Endocrine System. *Endocr Rev* 16:200-257.

Bouillon R, Verstuyf A, Verlinden L, Eelen G and Mathieu C (2003) Prospects for Vitamin D Receptor Modulators As Candidate Drugs for Cancer and (Auto)Immune Diseases. *Recent Results Cancer Res* 164:353-356.

Brunger AT, Adams PD, Clore GM, DeLano WL, Gros P, Grosse-Kunstleve RW, Jiang JS, Kuszewski J, Nilges M, Pannu NS, Read RJ, Rice LM, Simonson T and Warren GL (1998) Crystallography & NMR System: A New Software Suite for Macromolecular Structure Determination. *Acta Crystallogr D Biol Crystallogr* 54:905-921.

Choi M, Yamamoto K, Masuno H, Nakashima K, Taga T and Yamada S (2001) Ligand Recognition by the Vitamin D Receptor. *Bioorg Med Chem* 9:1721-1730.

Ciesielski F, Rochel N, Mitschler A, Kouzmenko A and Moras D (2004) Structural Investigation of the Ligand Binding Domain of the Zebrafish VDR in Complexes With 1 α ,25(OH)₂D₃ and Gemini: Purification, Crystallization and Preliminary X-Ray Diffraction Analysis. *J Steroid Biochem Mol Biol* 89-90:55-9.

Herdick M, Steinmeyer A and Carlberg C (2000) Antagonistic Action of a 25-Carboxylic Ester Analogue of 1 α , 25-Dihydroxyvitamin D₃ Is Mediated by a Lack of Ligand-Induced Vitamin D Receptor Interaction With Coactivators. *J Biol Chem* 275:16506-16512.

Issa LL, Leong GM, Sutherland RL and Eisman JA (2002) Vitamin D Analogue-Specific Recruitment of Vitamin D Receptor Coactivators. *J Bone Miner Res* 17:879-890.

Jones TA, Zou JY, Cowan SW and Kjeldgaard (1991) Improved Methods for Building Protein Models in Electron Density Maps and the Location of Errors in These Models. *Acta Crystallogr A* 47:110-119.

Makin G, Lohnes D, Byford V, Ray R and Jones G (1989) Target Cell Metabolism of 1,25-Dihydroxyvitamin D₃ to Calcitroic Acid. Evidence for a Pathway in Kidney and Bone Involving 24-Oxidation. *Biochem J* 262:173-180.

Otwinowski Z and Minor W (1997) Processing X-ray data collected in oscillation mode. *Methods Enzymol* 276:307-326.

Rachez C and Freedman LP (2000) Mechanisms of Gene Regulation by Vitamin D₃ Receptor: a Network of Coactivator Interactions. *Gene* 246:9-21.

Rachez C, Gamble M, Chang CP, Atkins GB, Lazar MA and Freedman LP (2000) The DRIP Complex and SRC-1/P160 Coactivators Share Similar Nuclear Receptor Binding Determinants but Constitute Functionally Distinct Complexes. *Mol Cell Biol* 20:2718-2726.

Rachez C, Lemon BD, Suldan Z, Bromleigh V, Gamble M, Naar AM, Erdjument-Bromage H, Tempst P and Freedman LP (1999) Ligand-Dependent Transcription Activation by Nuclear Receptors Requires the DRIP Complex. *Nature* 398:824-828.

Rachez C, Suldan Z, Ward J, Chang CP, Burakov D, Erdjument-Bromage H, Tempst P and Freedman LP (1998) A Novel Protein Complex That Interacts With the Vitamin D3 Receptor in a Ligand-Dependent Manner and Enhances VDR Transactivation in a Cell-Free System. *Genes Dev* 12:1787-1800.

Reddy GS, Rao DS, Siu-Caldera ML, Astecker N, Weiskopf A, Vouros P, Sasso GJ, Manchand PS and Uskokovic MR (2000) 1 α ,25-Dihydroxy-16-Ene-23-Yne-Vitamin D3 and 1 α ,25-Dihydroxy-16-Ene-23-Yne-20-Epi-Vitamin D3: Analogs of 1 α ,25-Dihydroxyvitamin D3 That Resist Metabolism Through the C-24 Oxidation Pathway Are Metabolized Through the C-3 Epimerization Pathway. *Arch Biochem Biophys* 383:197-205.

Reddy GS and Tserng KY (1989) Calcitroic Acid, End Product of Renal Metabolism of 1,25-Dihydroxyvitamin D3 Through C-24 Oxidation Pathway. *Biochemistry* 28:1763-1769.

Rochel N, Tocchini-Valentini G, Egea PF, Juntunen K, Garnier JM, Vihko P and Moras D (2001) Functional and Structural Characterization of the Insertion Region in the Ligand Binding Domain of the Vitamin D Nuclear Receptor. *Eur J Biochem* 268:971-979.

Rochel N, Wurtz JM, Mitschler A, Klaholz B and Moras D (2000) The Crystal Structure of the Nuclear Receptor for Vitamin D Bound to Its Natural Ligand. *Mol Cell* 5:173-179.

Schuster I, Egger H, Astecker N, Herzig G, Schussler M and Vorisek G (2001a) Selective Inhibitors of CYP24: Mechanistic Tools to Explore Vitamin D Metabolism in Human Keratinocytes. *Steroids* 66:451-462.

Schuster I, Egger H, Bikle D, Herzig G, Reddy GS, Stuetz A, Stuetz P and Vorisek G (2001b) Selective Inhibition of Vitamin D Hydroxylases in Human Keratinocytes. *Steroids* 66:409-422.

Takeyama K, Masuhiro Y, Fuse H, Endoh H, Murayama A, Kitanaka S, Suzawa M, Yanagisawa J and Kato S (1999) Selective Interaction of Vitamin D Receptor With Transcriptional Coactivators by a Vitamin D Analog. *Mol Cell Biol* 19:1049-1055.

Tocchini-Valentini G, Rochel N, Wurtz JM, Mitschler A and Moras D (2001) Crystal Structures of the Vitamin D Receptor Complexed to Superagonist 20-Epi Ligands. *Proc Natl Acad Sci U S A* 98:5491-5496.

Tocchini-Valentini G, Rochel N, Wurtz JM and Moras D (2004) Crystal Structures of the Vitamin D Nuclear Receptor Liganded With the Vitamin D Side Chain Analogues Calcipotriol and Seocalcitol, Receptor Agonists of Clinical Importance. Insights into a Structural Basis for the Switching of Calcipotriol to a Receptor Antagonist by Further Side Chain Modification. *J Med Chem* 47:1956-1961.

Toell A, Gonzalez MM, Ruf D, Steinmeyer A, Ishizuka S and Carlberg C (2001) Different Molecular Mechanisms of Vitamin D(3) Receptor Antagonists. *Mol Pharmacol* 59:1478-1485.

Uskokovic MR, Norman AW, Manchand PS, Studzinski GP, Campbell MJ, Koeffler HP, Takeuchi A, Siu-Caldera ML, Rao DS and Reddy GS (2001) Highly Active Analogs of 1 α ,25-Dihydroxyvitamin D(3) That Resist Metabolism Through C-24 Oxidation and C-3 Epimerization Pathways. *Steroids* 66:463-471.

Verlinden L, Verstuyf A, Quack M, Van Camp M, Van Etten E, De Clercq P, Vandewalle M, Carlberg C and Bouillon R (2001) Interaction of Two Novel 14-Epivitamin D3 Analogs With Vitamin D3 Receptor-Retinoid X Receptor Heterodimers on Vitamin D3 Responsive Elements. *J Bone Miner Res* 16:625-638.

Verlinden L, Verstuyf A, Van Camp M, Marcelis S, Sabbe K, Zhao XY, De Clercq P, Vandewalle M and Bouillon R (2000) Two Novel 14-Epi-Analogues of 1,25-Dihydroxyvitamin D3 Inhibit the Growth of Human Breast Cancer Cells in Vitro and in Vivo. *Cancer Res* 60:2673-2679.

Verstuyf A, Verlinden L, Van Baelen H, Sabbe K, D'Hallewyn C, De Clercq P, Vandewalle M and Bouillon R (1998) The Biological Activity of Nonsteroidal Vitamin D Hormone Analogs Lacking Both the C- and D-Rings. *J Bone Miner Res* 13:549-558.

Yamamoto H, Shevde NK, Warriar A, Plum LA, DeLuca HF and Pike JW (2003) 2-Methylene-19-nor-(20S)-1,25-Dihydroxyvitamin D3 Potently Stimulates Gene-Specific DNA Binding of the Vitamin D Receptor in Osteoblasts. *J Biol Chem* 278:31756-31765.

Footnotes

This work was supported by grants G.0242.01 and G.0150.02 from the Flemish Fund for Scientific Research (FWO) and by grants from CNRS, INSERM, Hôpital Universitaire de Strasbourg and Ministère de la Recherche et de la Technologie. This work benefits from the technical platform of structural genomics supported by the Genopole and SPINE programs. LV is a post-doctoral researcher from the FWO.

Corresponding author to whom reprint request should be addressed;

Roger Bouillon, PhD, MD

Laboratorium voor Experimentele Geneeskunde en Endocrinologie

Onderwijs en Navorsing, Gasthuisberg

Herestraat 49, B-3000 Leuven, Belgium

Tel.: +32-16-345970

Fax: +32-16-345934

E-mail: roger.bouillon@med.kuleuven.ac.be

Figure Legends

Fig 1. Chemical structure of 14-epi-analogs.

Fig 2. Effect of 1,25-(OH)₂D₃ and 14-epi-analogs on the interaction VDR – TIF2.

COS1 cells were transfected with pVPVDR, pGALTIF2.4 and the pG5CAT- reporter and treated with 1,25-(OH)₂D₃, TX522 and TX527 at the indicated doses or with vehicle. CAT-accumulation was normalized to total protein content and expressed as relative CAT amounts (RCA). Results shown are the mean ± SEM of at least three independent experiments performed in triplicate. ★ indicates RCA significantly different from RCA for 1,25-(OH)₂D₃-treated samples; p<0.05 according to Fisher's LSD multiple-comparison test.

Fig 3. Effect of 1,25-(OH)₂D₃ and 14-epi-analogs on the interaction VDR – SRC-1.

COS1 cells were transfected with pVPVDR, pSG424SRC1NIR and the pG5CAT-reporter and treated with 1,25-(OH)₂D₃, TX522 and TX527 at the indicated doses or with vehicle. CAT-accumulation was normalized to total protein content and expressed as relative CAT amounts (RCA). Results shown are the mean ± SEM of at least three independent experiments performed in triplicate. ★ indicates RCA significantly different from RCA for 1,25-(OH)₂D₃-treated samples; p<0.05 according to Fisher's LSD multiple-comparison test.

Fig 4. Effect of 1,25-(OH)₂D₃ and 14-epi-analogs on the interaction VDR –

DRIP205. COS1 cells were transfected with pVPVDR, pMDRIP205 and the pG5CAT-reporter and treated with 1,25-(OH)₂D₃, TX522 and TX527 at the indicated doses or with vehicle. CAT-accumulation was normalized to total protein content and expressed as

relative CAT amounts (RCA). A representative experiment of three independent experiments is shown. Data shown are the mean \pm SEM of triplicate samples. ★ indicates RCA significantly different from RCA for 1,25-(OH)₂D₃-treated samples; $p < 0.05$ according to Fisher's LSD multiple-comparison test.

Fig 5. Effect of the 24-hydroxylase inhibitor VID400 on VDR-DRIP205 interaction induced by 1,25-(OH)₂D₃ and 14-epi-analogs.

COS1 cells were transfected with pVPVDR, pMDRIP205 and the pG5CAT- reporter and treated with 1,25-(OH)₂D₃, TX522 and TX527 (10⁻⁹M) and with (black bars) or without (white bars) VID400 (2x10⁻⁷ M). CAT-accumulation was normalized to total protein content and expressed as relative CAT amounts (RCA). A representative experiment of three independent experiments is shown. Data shown are the mean \pm SEM of triplicate samples. ★ indicates significant difference between RCA of VID400-treated and vehicle-treated samples; $p < 0.05$ according to Fisher's LSD multiple-comparison test.

Fig 6. *In vitro* antiproliferative effect of 1,25-(OH)₂D₃ and 14-epi-analogs combined with VID400 on MCF-7 cells. [³H]-thymidine incorporation of MCF-7 cells incubated for 72h with 1,25-(OH)₂D₃, TX522 and TX527 at the indicated doses and with VID400 (2x10⁻⁷ M). A representative experiment of three independent experiments is shown. Data shown are the mean \pm SEM of samples assayed at least in triplicate.

Fig 7. Comparison of the ligand conformations of 1,25-(OH)₂D₃ (blue) and TX522 (green) in their VDR ligand binding pockets.

Fig 8. Superposition of the VDR-1,25-(OH)₂D₃ (yellow) and VDR-TX522 (blue) complexes. The view is restricted to the ligand binding pocket. Only residues closer than 4.0 Å are shown. The two residues Val300 and Ile268 making different contacts with

TX522 are highlighted in red. The ligands 1,25-(OH)₂D₃ and TX522 are shown in stick representation with carbon and oxygen atoms in gray and red, respectively. The hydrogen bonds are shown as red dashed lines.

Table 1: Data collection and refinement statistics:

Ligand complexes	TX522
X-ray source	BM14
Wavelength (Å)	0.918
Cell (Å) ($\alpha=\beta=\gamma=90^\circ$)	a = 45.233 b = 52.437
Space group P2 ₁ 2 ₁ 2 ₁	c = 132.957
Resolution (Å)	25.0 – 1.84
(last shell)	(1.88 – 1.84)
Unique reflexions	26792
Redundancy	3.6
Completeness (last shell) (%)	99.0 (98.0)
R _{sym} (last shell) (%)	5.0 (26.2)
I/σ(I) (last shell)	17.5 (3.6)
R _{cryst} (%)	18.8
R _{free} (%)	21.6
Rmsd bond length (Å)	0.0049
Rmsd bond angles (°)	1.05
Number of non-hydrogen protein atoms	2013
Number of non-hydrogen ligand atoms	30
Number of water molecules	135
B _{avg} (Å ²) protein atoms	20.2
B _{avg} (Å ²) ligand atoms	15.1
B _{avg} (Å ²) water molecules	33.4

Fig. 1

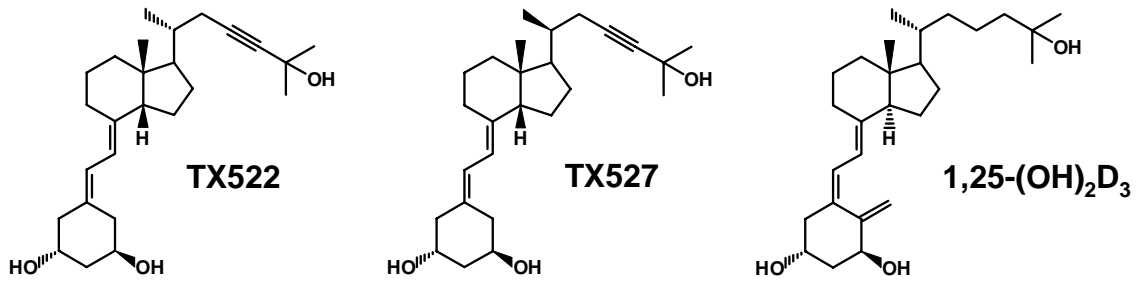


Fig. 2

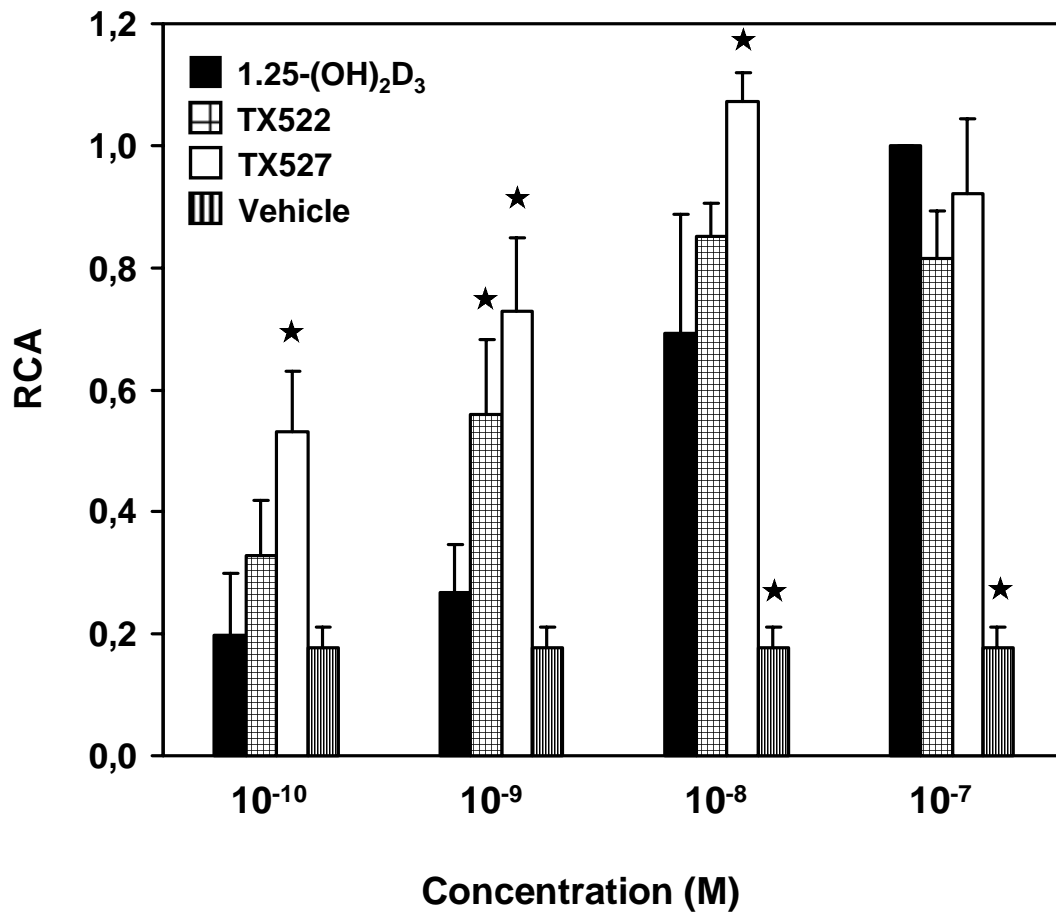


Fig. 3

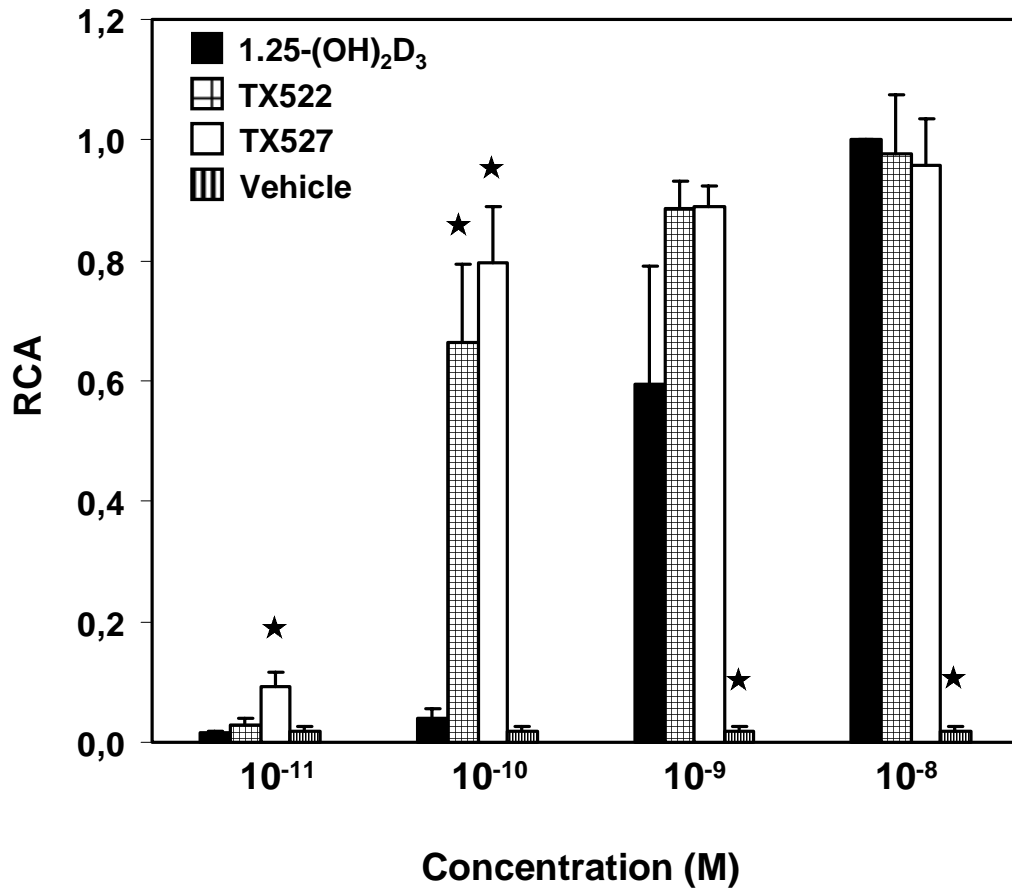


Fig. 4

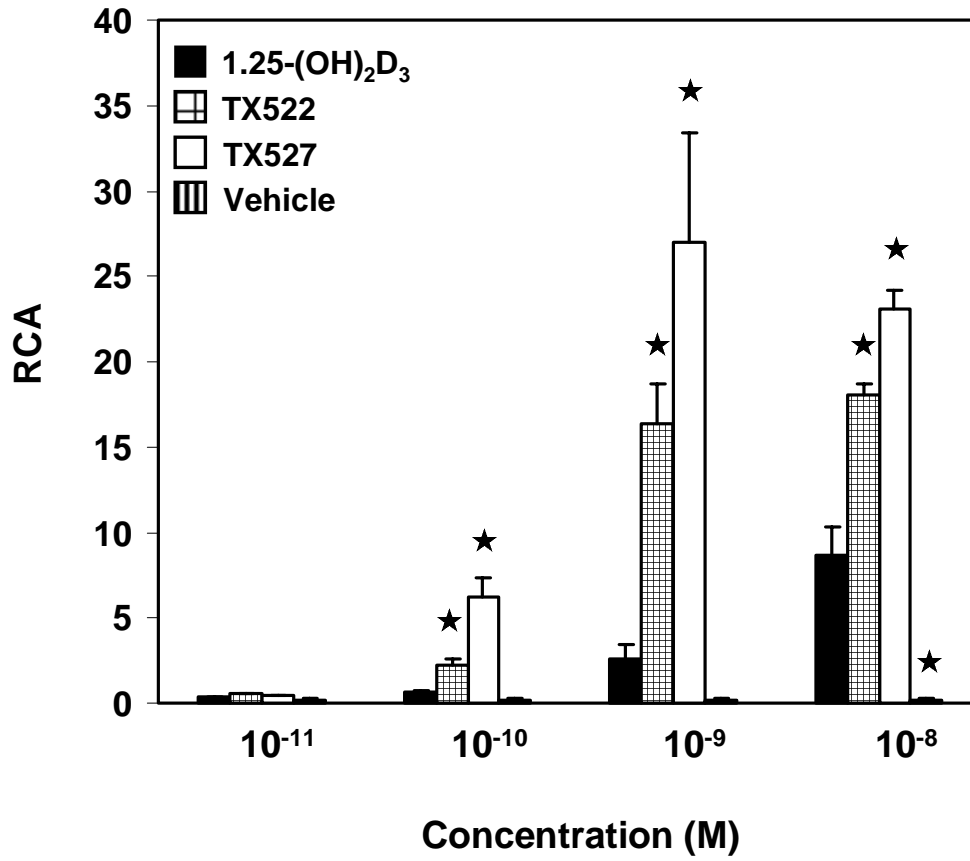


Fig. 5

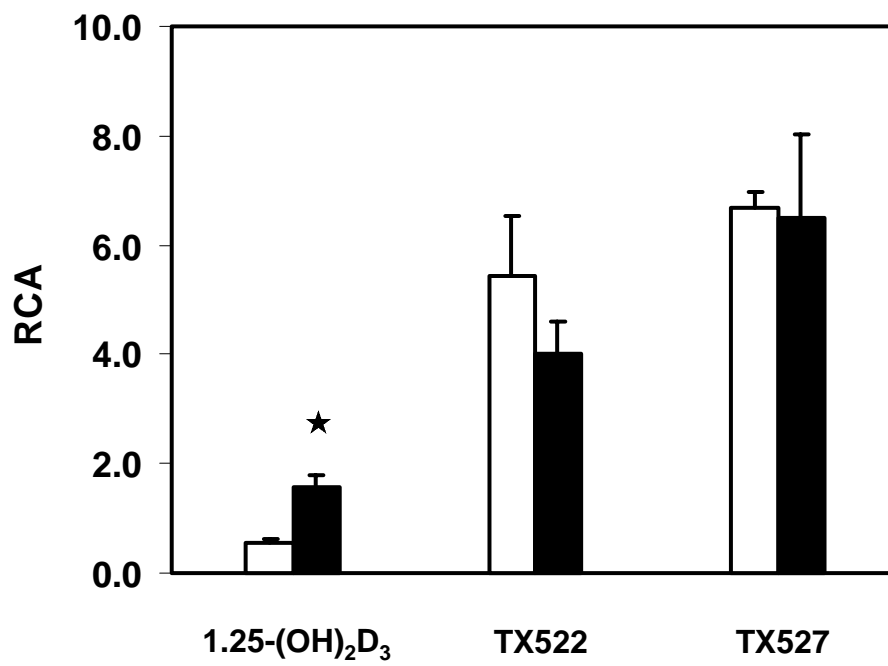


Fig. 6

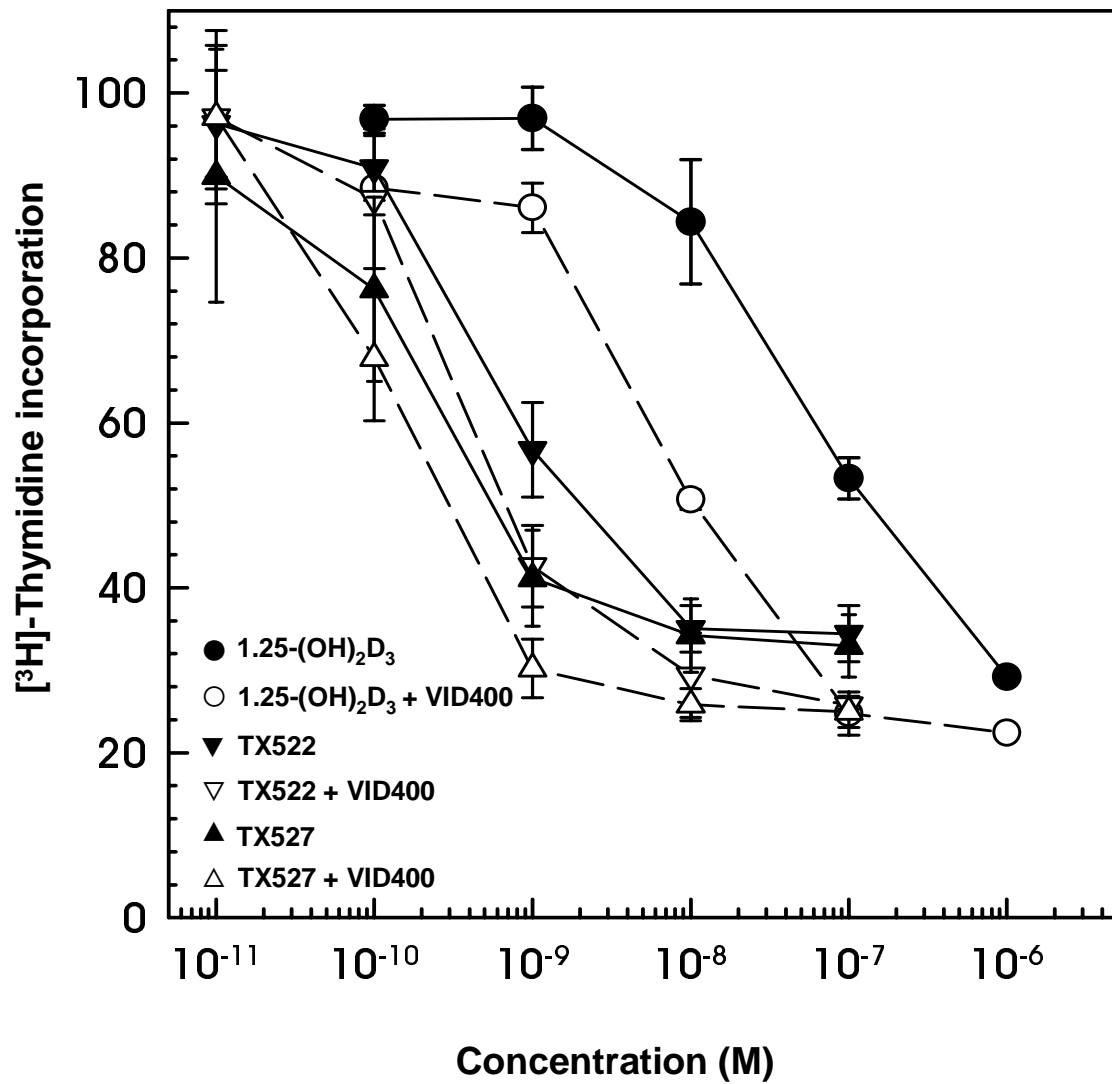


Fig. 7

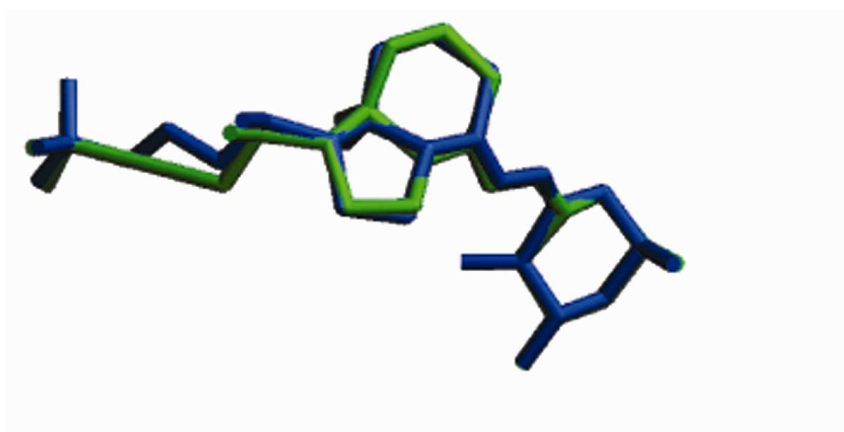


Fig. 8

